Contents lists available at ScienceDirect

Talanta

journal homepage: http://ees.elsevier.com

Quantification of manganous ions in wine by NMR relaxometry

Philippe R. Bodart [a,b,*], Adam Rachocki [c], Jadwiga Tritt-Goc [c], Bernhard Michalke [d], Philippe Schmitt-Kopplin [d,e], Thomas Karbowiak [a], Regis D. Gougeon [a]

[a] Univ. Bourgogne Franche-Comté, Agrosup Dijon, UMR PAM A02.102, 1 Esplanade Erasme, 21000, Dijon, France
[b] IUT A - Université des Sciences et Technologies de Lille, Villeneuve d'Ascq, 59655, France
[c] Institute of Molecular Physics, Polish Academy of Sciences, M. Smoluchowskiego 17, 60-179, Poznan, Poland
[d] Research Unit Analytical BioGeoChemistry, Department of Environmental Sciences, Helmholtz Zentrum München, Ingolstaedter Landstrasse 1, Neuherberg, 85764, Germany
[e] Chair of Analytical Food Chemistry, Technische Universität München, Alte Akademie 10, 85354, Freising-Weihenstephan, Germany

ARTICLE INFO

Keywords
FFC NMR relaxometry
Wine
Paramagnetic ions
Manganese

ABSTRACT

Proton relaxation in model and real wines is investigated for the first time by fast field cycling NMR relaxometry. The relaxation mechanism unambiguously originates form proton interaction with paramagnetic ions naturally present in wines. Profiles of a white Chardonnay wines from Burgundy, a red Medoc, and model wines are well reproduced by Solomon-Bloembergen-Morgan equations. Relaxation is primarily governed by interactions with Mn^{2+}. A straightforward model-independent quantification of the manganese ion concentration (down to few tens of μg/L) is proposed.

1. Introduction

Since the pioneering work of Eschnauer on trace elements [1,2], there has been a wealth of scientific publications tracing the various contributions throughout the overall winemaking process, from the vineyard to the ageing in bottles, which may have an impact on the transient concentrations of elements in grape and ultimately in wine [3–7]. Besides, multi-elemental fingerprinting has further proven to be a promising wine authentication strategy [8–10], although only recent studies have investigated the interplay between the winemaking processes and the viticultural origin of the grapes on the actual composition of wines [11]. Of all the elements present in wines, transition metals and in particular Fe and Cu have been the subject of many studies, since these two cations, with Mn to a lesser extent, were shown to play a central role in catalyzing oxidation [12,13]. Considered as natural elements in wine, whose presence is the result of a plant uptake from the soil [6], Fe, Cu, Mn, and also Ni, can be incorporated during winemaking, as a result of "contamination" from winery equipment or as a consequence of practices such as clarification and filtration [3,14]. Nevertheless, and despite the fact that the successive winemaking steps can modulate concentrations [5]; these four elements could be considered as discriminant among different Australian wine regions [15].

Although alternative methodologies such as near infrared spectroscopy were proposed for the analysis of elements in wine [16], their quantification mostly relies on atomic spectroscopy techniques, and in particular on inductively coupled plasma optical emission spectroscopy (ICP–OES), and mass spectrometry (ICP–MS). Many elemental analyses over the last decades have involved, and are still based on such techniques [9,17–20]. They can achieve very high selectivity and sensitivity, with reduced problems of interference due to matrix effects, but rely on expensive equipment. Furthermore, when dealing with biological samples like wine, metal speciation is a critical issue, and the association of ICP-OES with fractionation strategies such as solid phase extraction has recently been used to discriminate Cu and Fe as hydrophobic, cationic and residual [13]. Besides, colorimetric or electrochemical methods have also been used for Cu and Fe speciation in wine [21].

To our knowledge, fast field cycling (FFC) NMR relaxometry has never been used to characterize wine and this preliminary communication aims to determine the origin of NMR relaxation in wine and to highlight some major information that could be extracted. FFC NMR relaxometry is the only low-field NMR technique that measures the longitudinal, or spin lattice relaxation time (T1), as a function of the magnetic field strength, over a wide range of frequencies (from a few kHz to tens of MHz) corresponding to values of T1 in the order of seconds to a fraction of a millisecond. Data are displayed in the form of a nuclear magnetic resonance dispersion (NMRD) profile, where the relaxation rate (R1 = 1/T1) is reported versus the Larmor frequency of the observed nuclei. Generally, the benefit of exploring the nuclear spin-lattice relaxation rate over a large range of frequencies is to isolate the

* Corresponding author. Univ. Bourgogne Franche-Comté, Agrosup Dijon, UMR PAM A02.102, 1 Esplanade Erasme, 21000, Dijon, France.
E-mail address: Philippe.bodart@u-bourgogne.fr (P.R. Bodart)

https://doi.org/10.1016/j.talanta.2019.120561
Received 12 June 2019; Received in revised form 2 November 2019; Accepted 11 November 2019
Available online xxx
0039-9140/

typical NMRD features associated with different molecular dynamics. Varying the magnetic field (B_o) changes the Larmor frequency ($\nu_o = \gamma B_o/2\pi$, where γ is the gyromagnetic ratio of the observed nuclei) and therefore the time and length scales of the fluctuations responsible for the nuclear spin-lattice relaxation rate R1 [22–24]. It is possible to record NMRD profile of almost any material, solid, liquid, or colloid. In food science, FFC NMR has been applied to seeds [25], oil [26–28], fruits [29–31], cacao butter [32,33], starch [34], bread [35], honey [36,37], egg and meat [38–40], cheese [41], quality and anti-fraud controls [42]. The art of exploiting NMRD profile consists in finding a sensible model in the sense that it describes correctly the fluctuation of the NMR interactions. It requires a very good knowledge of the system studied which is for the less no obvious in many complex food systems.

2. Materials and methods

2.1. Field cycling NMR relaxometry

Proton spin–lattice relaxation measurements were performed on a field cycling relaxometer from Stelar company (Mede, Italy) with a magnetic field B_o, covering the proton Larmor frequencies from 0.001 to 40 MHz [43–45]. The spectrometer operates by switching the current in a solenoidal magnet from a polarizing field (B_{pol}), corresponding to a proton Larmor frequency of 24 MHz, to a field of interest (B_{rel}) for a variable relaxation period (τ). After each τ delay, the B_{rel} field is switched to the acquisition field (B_{acqu}), corresponding to a proton Larmor frequency of 16 MHz, at which magnetization is detected after a $\pi/2$ pulse. The measurements were carried out at a temperature of 25 °C, 4 scans were recorded, $\pi/2$ pulse was 10 μs, the field-switching time 3 ms, spectrometer dead time 18 μs, and spectral width 1.25 MHz. Points number 5 to 50 of fids were added to produce the relaxation curves, a single exponential relaxation curve was observed in each experiment and the decay/recovery curves at each B_{rel} value were fitted, using a single exponential function.

2.2. NMR titrations

Metal titration curves were recorded at 25 °C on a minispec mq20 (Bruker) operating at 19.65 MHz. Four scans were collected and experiments were repeated at least 4 times. Relaxation time T1 was measured with an inversion recovery pulse sequence. A single exponential relaxation curve was observed in each experiment.

2.3. Inductively coupled plasma atomic emission spectrometry

An ICP-AES Spectro ARCOS system (SPECTRO Analytical Instruments GmbH & Co. KG, Kleve, Germany) was used for a complete screen of elements. The measured spectral element lines were: Cu: 324.754 nm, Fe: 259.941 nm, Mn: 257.611 nm, Mo: 202.030 nm, Ni: 231.614 nm. Sample introduction was carried out using a peristaltic pump connected to a Meinhard nebuliser with a cyclon spray chamber. The RF power was set to 1250 W, the plasma gas was 15 L Ar/min, whereas the nebuliser gas was 0.6 L Ar/min. After 1:20 dilution of the samples with Milli-Q H_2O for providing enough sample volume for measurements (only few μL had been available) they were directly analyzed. As a positive side effect the dilution eliminated probably occurring matrix effects and sensitivity changes due to ethanol from samples.

2.4. Samples

A Chardonnay white wine (2014 vintage) from the University of Burgundy estate in Marsannay-la-Côte, Côte d'Or, France (samples W), and a red Medoc blend wine (2011 vintage) from Bordeaux (samples R) were selected for real wine analysis. A label (a or b) indicate that the experiment has been performed with the sample as received (Ra, Wa) or one year latter (Rb,Wb). The exchanged wine (EW) was produced by exchange of W on an acidic cation exchange resin: Dowex 50WX8-100 (capacity 1.7 meq. mL^{-1}; Sigma–Aldrich), adapted from the procedure of Benitez [46]. The resin was activated with 10% HCl and washed with Milli-Q water until the eluate was neutral. Then, 20 mL W were mixed with 0.3 g of activated resin under stirring for 10 min. After filtration of the mixture on a 0.65 mm cellulose acetate membrane, the filtrate was stored at 4 °C until analysis.

Ethanol (198.85 g, Aldrich ≥ 99.9%) was added to 1497.3 g of ultra-pure water with 7.5 g of citric acid to produce a 12% (vol) model wine. Anhydrous paramagnetic salts FeCl3 and $CuSO_4$ (Aldrich ≥ 99.99%), were used as received. $FeSO_4.7H_20$ (Sigma ≥99.99) was also used as received, but the solute (water or hydro alcoholic solution) was degassed under N_2 (down to an oxygen concentration of 0.5 mg/L) prior addition of the salt. $MnSO_4.xH_20$ (Aldrich ≥ 99.99) was heated at 450 °C during 14 h to remove residual water [47,48]. $NiCl_3.6H_20$ (Fluka >98.0%) was heated at 220 °C for 10 h to produce anhydrous chloride. Stock solutions of 50 mg/L of paramagnetic ions were diluted to obtain targeted titration solutions. Laboratory glassware was cleaned three times with MilliQ water and ultrapure water prior syntheses of model wine used for the titration curves with Mn^{2+}, Ni^{2+}, Cu^{2+}, Fe^{2+}, and Fe^{3+}. The pH of model wines was 3.5, while white and red wine pH were 3.3 and 3.7 respectively. Samples are labelled MWx for Model Wine containing x/100 mg/L of manganese (i.e. MW005 contains 0.05 mg/L of manganese).

4. Theoretical description

Any nucleus experiencing a space-dependent NMR interaction can generate a path for magnetic relaxation through the modulation of this interaction induced by nuclei dynamic. Modelling of relaxation profiles is not straightforward, and we only refer to the most simple and commonly-used models. In the case of proton NMR relaxometry of a solution, the first interaction to consider is the dipolar interaction between protons. At equilibrium, isolated ^{1}H nuclear spins placed in a magnetic field *Bo* occupy two energy levels $\pm h\nu_o/2$ whose population is given by the Boltzmann distribution [49]. The unequal population of these two levels induces the *Bo*-proportional magnetization observed in NMR. In relaxation experiments, the sample, initially polarized in a strong external magnetic field (B_{pol}), is exposed to a lower relaxation magnetic field (B_{rel}), and the energy level populations are modified according to the second magnetic field. The magnetization has to relax in time, reaching eventually equilibrium at the lower field B_{rel}[23,50]. The magnetization decay is generally exponential with a time constant referred to as the spin-lattice relaxation time T1. The simplest description of relaxation mechanisms results from the stochastic fluctuations of dipolar interactions between pairs of proton of the same molecule [49]. This intramolecular relaxation is associated with molecular rotation changing the orientation of the vector connecting the interacting nuclei (within a molecule) with respect to the direction of the external magnetic field (rotational diffusion model). The relaxation rate depends on the spectral density of this fluctuation and if Lorentzian spectral densities are considered, it can be simply expressed as the Bloembergen-Purcell-Pound (BPP) model. In the case of two identical spins it is written [24,51]:

$$\widetilde{R}\left(\omega_I, \tau_o\right) = \widetilde{C}_o \left[\frac{\tau_o}{1+\left(\omega_I \tau_o\right)^2} + \frac{4\tau_o}{1+4\left(\omega_I \tau_o\right)^2} \right] \quad (1)$$

With:

$$\widetilde{C}_o = \frac{3}{10}\left(\frac{\mu_o}{4\pi}\right)^2 \frac{\gamma_I{}^4 \hbar^2}{r_{II}{}^6} \quad (2)$$

where ω_I is the Larmor pulsation of the observed nuclei (^{1}H), τ_o is the

rotational correlation time, r_{II} is the distance between the two nuclei within the molecules, and the tilde accent specifies a two-spin interaction.

Paramagnetic relaxation is another, very efficient, relaxation mechanism resulting from the coupling between protons and unpaired electrons of any paramagnetic element. In particular, trace level of paramagnetic agents containing single ions are very effective relaxing agents in solution [52], and relaxometry has proven to be an efficient technique for various paramagnetic titrations [53–59].

Paramagnetic interactions are described by several mechanisms. The simplest one considers that the unpaired electrons are localized at the paramagnetic ion. The relaxation is described by an interaction between an electronic point dipole and a nuclear point dipole (Solomon mechanism).

The associated dipolar paramagnetic relaxation rate can be written in the case of two spins as [60–64]:

$$\widetilde{R}_D\left(\omega_I, \tau_{d1}, \omega_s, \tau_{d2}\right) = \widetilde{C}_D\left[\frac{7\tau_{d2}}{1+\left(\omega_s\tau_{d2}\right)^2} + \frac{3\tau_{d1}}{1+\left(\omega_I\tau_{d1}\right)^2}\right] \quad (3)$$

With

$$\widetilde{C}_D = \frac{2}{15}\left(\frac{\mu_o}{4\pi}\right)^2 \frac{S(S+1)\left(\gamma_I\,\gamma_S\hbar\right)^2}{r_{IS}{}^6} \quad (4)$$

where S is the electron spin number of the paramagnetic ion, and S-subscript refers to paramagnetic ion. Correlation time τ_{di} is a composition of the reorientational correlation time of the paramagnetic ion (τ_R) due to Brownian rotational motion, longitudinal (i = 1) or transverse (i = 2) electron relaxation time (τ_{Si}), and of the life time of the nuclei on the paramagnetic ion (τ_M):

$$\frac{1}{\tau_{di}} = \frac{1}{\tau_R} + \frac{1}{\tau_M} + \frac{1}{\tau_{Si}} \quad (5)$$

in practice, at low magnetic field, $\tau_{d1} = \tau_{d2} = \tau_d$[64].

Equation (3) evidences two dispersions that can be observed at different frequencies. In low viscosity solutions at room temperature, the first term in bracket of equation (3) is responsible, for certain aquaions (e.g., Cu^{2+} [62,64,66], Mn^{2+} [62,64,66,67], Fe^{3+} [62,64,68], Gd^{3+} [64,69], Cr^{3+} [62,65]), for an inflection in the NMRD profile near 10 MHz ($\omega_s\tau_{d2} \sim 1$), τ_R . while other aquaions (e.g., Fe^{2+} [62], Co^{2+} [62], Ni^{2+} [70]) do not show any dispersion below 40 MHz. Since $\omega_S = 658\omega_I$ [64], the second term ($\omega_I\tau_{d1}$) of equation (3) induces a dispersion at a significantly higher frequency, in the GigaHertz range (the same remark holds for equation (1)). The characterization and discrimination of these high frequency dispersions requires data collected at magnetic fields significantly higher than the 500 MHz frequency used in this study. It must be pointed out that these considerations may be very different in other conditions (high viscosity, high temperature) or systems (e.g. in macromolecules the $\omega_I\tau_{d1}$ dispersion may appear below 50 MHz [71–76]).

The Solomon mechanism is not always sufficient to reproduce the NMRD profiles. In particular, in the case of the paramagnetic nuclei present in wines, an additional fermi-contact interaction (Bloembergen mechanism) has to be considered. This interaction arises from a delocalization of the electronic wave function of the paramagnetic nuclei to the physical location of I-nuclei.

The relaxation rate in the case of two spins experiencing a contact interaction (scalar or hyperfine interaction) is given by [61–64]:

$$\widetilde{R}_C\left(\omega_s, \tau_c\right) = \widetilde{C}_C\left[\frac{\tau_c}{1+\left(\omega_s\tau_c\right)^2}\right] \quad (6)$$

with:

$$\widetilde{C}_C = \frac{2A^2S(S+1)}{3\hbar^2} \quad (7)$$

where A is the scalar coupling constant of the spin exchange interaction between nucleus and electron, and τ_c is given by:

$$\frac{1}{\tau_c} = \frac{1}{\tau_M} + \frac{1}{\tau_{S2}} \quad (8)$$

Several aquaions (e.g., Fe^{3+} [62,68], Cr^{3+} [62,65], VO^{2+} [62,77]) experience this contact interaction, the associated dispersion in low viscosity solutions at room temperature is then situated at frequencies above 1 MHz. Manganous aquaions also experience a contact interaction with a characteristic low-field dispersive contribution (around 100 kHz) in the associated NMRD profile. Once more, in other conditions or systems, the previous consideration may be different.

Paramagnetic longitudinal relaxivity of the water protons (R_1^p) is given by [64,78]:

$$\frac{pq}{R_1^p} = \frac{1}{\widetilde{R}_D + \widetilde{R}_C} + \tau_M \quad (9)$$

where p is the concentration of the ions relative to the concentration of the solvent molecules (water) and q the number of metal-bound water molecules. Assuming a fast chemical exchange of the water molecules ($\tau_M \ll 1/\left(R_D + R_C\right)$. The relaxation of the water proton can be written:

$$R_1 = R + R_1^p = R + pq\left(\widetilde{R}_C + \widetilde{R}_D\right) = R + R_D + R_C \quad (10)$$

where R can be associated to the background or solvent rate in the absence of paramagnetic ions, R_D and R_C are the dipolar and contact paramagnetic contribution from the exchange of solvent nuclei with the hydrated paramagnetic ions (first sphere of coordination). The contributions from second sphere and longer range paramagnetic interactions are not considered here. When different types of solute paramagnetic ions are present, the contributions R_C and R_D of independent relaxation processes can be treated as additive [64], and (10) can be extended as:

$$R_1 = R + R_C^{Mn(II)} + \sum_{i\neq Mn} R_C^i + \sum_i R_D^i \quad (11)$$

where i stands for all paramagnetic nuclei in the solution, $R_C^{Mn(II)}$ is explicitly reported to highlight the distinctive dispersion at ~0.1 MHz in wines at room temperature.

Detailed formalisms and more sophisticated developments can be found in reviews presenting theoretical description of paramagnetic NMR [52,63], but such developments are clearly beyond the scope of this communication.

5. Results and discussion

5.1. Wine NMRD profiles

Beside NMRD profiles of model wines (MW samples), profiles of two distinct wines: a white Chardonnay from Burgundy (W samples) and a red Medoc blend (R samples) were also recorded. Samples were analyzed at two different times: as received in 2017 (Wa and Ra samples) and after one year exposed to atmospheric air in a closed NMR tube (ratio wine/air volume of 1/20; Wb and Rb samples). In wine, naturally present paramagnetic ions have low (mg/L) or very low (μg/L) concentrations, typical orders rarely exceed 5 mg/L for iron, 2 mg/L for

manganese, and are less than 1 mg/L for copper [5]. ICP-AES analyses of our samples are reported in Table 1.

To test paramagnetic relaxation mechanism in wine, Fig. 1 reports NMRD profiles of the white wine recorded before (Wa) and after (EW) ion exchange treatment on a resin to remove paramagnetic ions [46]. When paramagnetic ions are extracted from the wine, a featureless profile with longer relaxation times is observed, confirming the dominant paramagnetic relaxation mechanisms in wine. Moreover, in Wa profile, the low frequency dispersion around 0.1 MHz is characteristic of manganese, and in a first approximation proton coupling with manganese has to be assumed. For comparison, the NMRD profiles of two model wines (MW005 and MW128) solely containing manganese as paramagnetic ions at levels of 50 μg/L and 1.28 mg/L and the profile of the red wine are reported in Fig. 1.

Table 1
Concentrations (mg/L) of paramagnetic elements measured in the white Chardonnay (W), the red Medoc (R) and the exchanged wine (EW) by ICP-AES. Numbers in parentheses are the uncertainties on the last digits.

	Mn	Fe	Cu	Ni	Cd
W	1.26 (2)	1.34 (2)	0.160 (2)	0.91 (1)	0.0019 (1)
EW	<0,002	0.056 (3)	0.024 (1)	<0,007	<0,001
R	1.06 (2)	0.85 (1)	0.93 (1)	0.065 (1)	0.0056 (3)

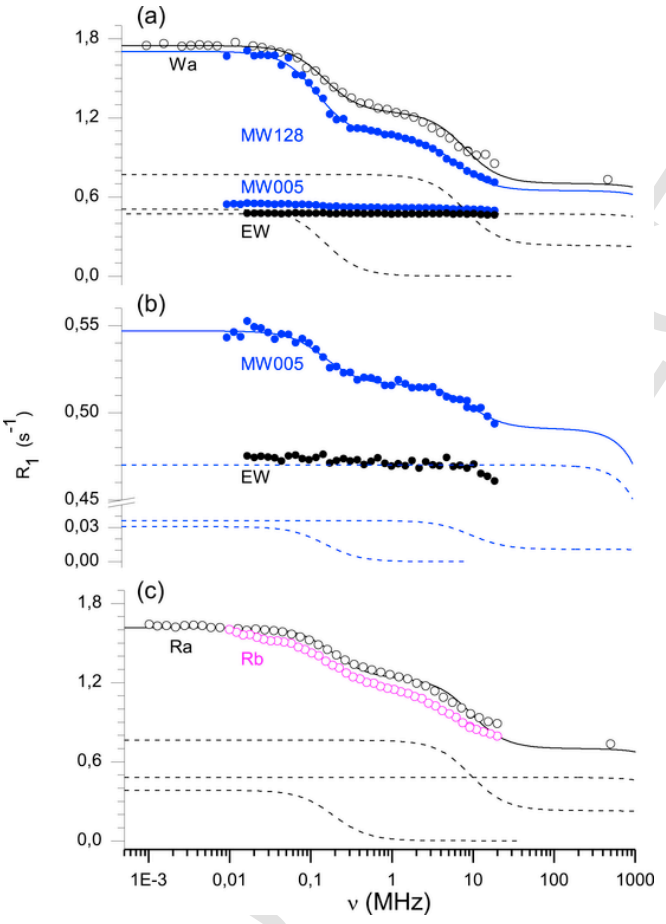

Fig. 1. NMRD profiles of real and model wines. Black and pink symbols represent profiles of real wine (Wa, Ra, ○; Rb, ○) and exchanged wine (EW, ●). Blue symbols report profile of synthetic wine MW005 (50 μg/L Mn2+) and MW128 (1.28 mg/L Mn2+). Continuous lines result from the refinement of real and model wines, individual components of the fits are represented by dashed lines. (a) white wine Wa, EW, MW005, and MW128. (b) vertical extension of the profile of MW005 with its refinement and related components along with the EW profile. (c) Red wines, with Ra refinement . The profile of Wb overlaps Wa one's and is not reported. (For interpretation of the references to color in this figure legend, the reader is referred to the Web version of this article.)

The shapes of the real and model wine profiles are similar. Furthermore, the clear manganese fingerprint characterized by two dispersions around 0.1 and 10 MHz observed in MW005, indicates that 50 μg/L is clearly above the limit of detection and quantification. In Fig. 1, NMRD profiles are satisfactory reproduced with the following equation:

$$R_1 = R(\omega_I, \tau_o) + R_D(\omega_I, \omega_s, \tau_d) + R_C(\omega_s, \tau_c) \quad (12)$$

Numerical parameters resulting from the refinement are gathered in Table 2 with additional results from wines and model wines containing 5.43 (MW543), 5.01 (MW501), and 0.53 (MW053) mg/L of Mn^{2+}. Since we do not have high frequency data to refine the diamagnetic contribution (equation (1)), the relaxation rate of the model wine without paramagnetic elements measured at 20 MHz (0.47 s^{-1}) was used to fix the diamagnetic contribution $(R(\omega_I, \tau_o))$.

In Table 2, correlation times τ_d and τ_c are consistent with literature data of Mn^{2+} in solution [62,64,67,77,79]. Among model wine samples, little deviations are observed, the somehow lower correlation times measured for MW005 may simply result from the noisier data. However, the measured dipolar values differ notably between the two red wines. In fact, an inspection of samples Ra and Rb revealed that, while Ra had a natural red color, Rb turned very brown indicating a contact with air. This air-contact, among various changes in the wine, induces oxidation and eventually evaporation of alcohol, which contribute to a decrease of the relaxation rate (Fig. 4). The signature of this oxidation is already observable on Ra and Rb profiles (Fig. 1c), Rb curve is downward-shifted with respect to that of Ra (~0.1 s^{-1}at 20 MHz). The refinement of the profiles is performed with a diamagnetic contribution fixed to 0.47 s^{-1} which is of course unappropriated in the case of Rb and the 0.1s^{-1} shift is numerically reported in the C_D parameter.

Variation of parameters C_D and C_C versus the manganese concentration for the model wines is reported in Fig. 2.

The C_C parameter results from the contact interaction proper to Mn^{2+}, therefore a report of C_C obtained from Wa NMRD profile, on the line of Fig. 2 gives a measure of the manganese concentration in the wine: 1.26 ± 0.08 mg/L . Results obtained for other samples are reported in Table 3, the relaxation measurement of the manganese concentration agrees with the ICP-AES analysis, confirming the major role of manganese in the paramagnetic relaxation mechanism.

The dispersion around 10 MHz can be affected by the dipolar or contact interactions of other paramagnetic elements present in the wine (Fe [62,66], Cu [62]) and the report of C_D on Fig. 2 can overestimate the Mn^{2+} concentration. Dispersions from other paramagnetic nuclei

Table 2
Parameters obtained from refinements of NMRD profiles for the white Chardonnay (W), the red Medoc blend (R) and model wines (MW). MWx refers to model wines containing x/100 mg/L of manganese. $C_{D/C} = pq\tilde{C}_{D/C}$ and numbers in parentheses are last-digit-uncertainties resulting purely from the numerical refinement.

	R_D		R_C	
	C_D (10^9 s^{-2})	τ_d(10^{-11}s)	C_C (10^9 s^{-2})	τ_c(10^{-9} s)
MW546	5.78	3.81 (2)	1.41	1.88 (1)
MW501	5.47	3.78 (2)	1.27	1.86 (2)
MW128	1.64	3.60 (3)	0.34	1.87 (3)
MW053	0.72	3.43 (3)	0.14	1.82 (3)
MW005	0.25	1.80 (2)	0.02	1.50 (4)
Wa	2.73	2.82 (3)	0.33	1.51 (3)
Wb	2.69	2.92 (2)	0.36	1.43 (2)
Ra	2.97	2.56 (2)	0.30	1.28 (3)
Rb	2.07	3.22 (3)	0.30	1.38 (4)

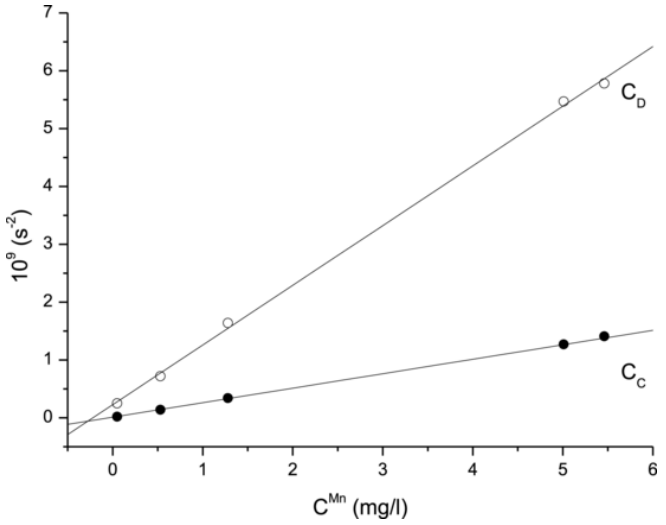

Fig. 2. Variation of C_C and C_D parameters versus manganese concentration for the model wines.

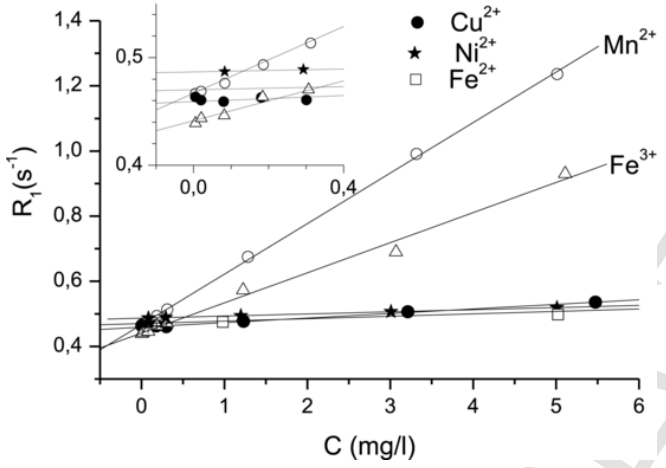

Fig. 3. Proton relaxation rates of model wines versus metal concentration, recorded at 19.65 MHz. Continuous lines correspond to linear regressions. For linear regressions of model wines containing Ni^{2+}, Cu^{2+}, and Fe^{2+} relaxation times of wines with 50, 25 and 10 mg/L have been measured (data not shown).

are also the probable explanation for the mismatch of the simulated profiles and the experimental points around 10 MHz. Furthermore, they may as well contribute to the differences observed around 10 MHz between the profiles of model wine MW128 and Wa, which have very close Mn^{2+} concentrations and should match once vertically shifted (Fig. 1a). Since the wines contain several paramagnetic elements (Table 1), it is important to examine how the other paramagnetic nuclei could contribute to the relaxation of the wine, and be observed in the NMRD profiles.

Fig. 3 reports the relaxation rates recorded at a Larmor frequency of 19.65 MHz measured on model wines containing variable amount of paramagnetic nuclei present in the wines (Cu^{2+}, Fe^{2+}, Mn^{2+}, Ni^{2+}, Fe^{3+}). Intercepts, and slopes (proton relaxivities) of the linear correlations and some related literature values are reported in Table 4.

Comparable linear correlations have been reported for T1 and T2 relaxations for various paramagnetic ions in solution [57,58,80,82,87]. The curves intercept the y-axis at a value, which would be the relaxation rate of the model wine free of paramagnetic element (R_0), which can thus be considered as the solvent relaxation rate. Relaxivities of Fe^{2+}, Ni^{2+}, and Cu^{2+} ions are at least one order of magnitude inferior to the Mn^{2+} one and are not expected to signifi-

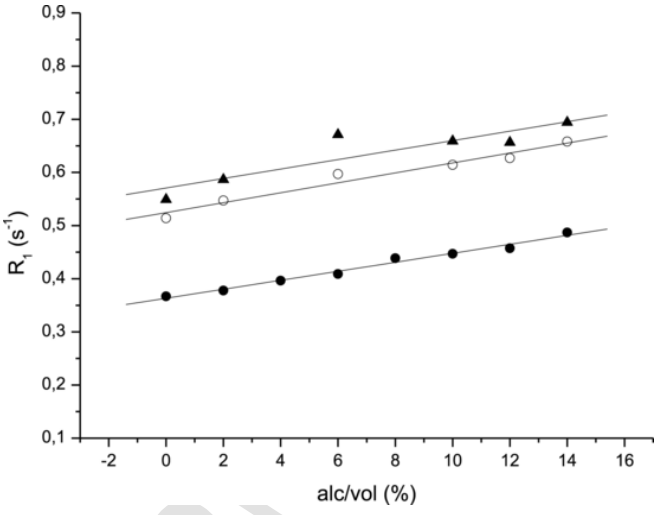

Fig. 4. Relaxation rate of alcoholic solutions, (●) Hydro-alcoholic solution, (○) alcoholic solution with 1.2 mg/L of Mn2+, and (▲)alcoholic solution containing 1.23 mg/L of manganese and 5 g/L of tartaric acid, versus the alcohol percent in volume (alc/vol) at 25 °C.

Table 3
Manganese concentrations (mg/L) in wine samples measured by ICP-AES and relaxometry. Concentrations reported in column C are calculated through the contact constant of the Solomon-Bloembergen-Morgan equation. Numbers in parentheses are uncertainties on the last digits.

	ICP-AES	C
Wa	1.26 (2)	1.26 (8)
Wb		1.38 (8)
Ra	1.06 (2)	1.15 (8)
Rb		1.13 (8)

cantly participate to the dipolar dispersion. Ferric aquaion which has a dispersive component around 7 MHz [62,68] is the only candidate that could contribute to the dipolar paramagnetic relaxation. This is a very interesting point that relaxometry could highlight in situ. Indeed, iron plays a determinant catalytic role in oxidation mechanism of wine. However, because of the tens of thousands of molecules and elements present in wine, oxidation mechanisms are very complex and have been the subject of numerous works [88–95]. It is well known that when wine is preserved from oxygen, iron is preferably in ferrous state and should therefore not contribute significantly to the relaxation. However, in the presence of O_2, it is oxidized to Fe^{3+} and it has been shown in real wines that Fe^{2+} concentration can decrease by 40–50% in 80 h after exposure to air [96]. Fe^{3+} is very likely to occur in our samples and increase the observed dispersion at 10 MHz. When oxidation processes are completed, Fe^{3+} can be reduced or form complexes and insoluble particles (i.e. $Fe(OH)_3$) that contribute to a lesser extent to the relaxation [54,56,59]. ICP-AES analysis of exchanged wine (EW), has revealed Mn^{2+}concentration below 0.002 mg/L. In Fig. 1, the NMR profile of EW shows a barely visible decreasing slope of the relaxation rate but no clear manganese signature is visible. A few μg/L of Mn^{2+} would be the limit of detection, at least within our experimental conditions. It is worth noting that in other systems (such as wine vinegars), profiles may show different paramagnetic signatures as a hump at high frequency [42,52,63,75]resulting from the formation of

Table 4
Proton relaxivity (r) and intercept (R_0) of model wines and water solutions containing metal ions (Mn^{2+}, Fe^{3+}, Fe^{2+}, Ni^{2+} and Cu^{2+}). If not specified otherwise, measurements were performed at 19.65 MHz and at 25 °C. Numbers in parenthesis indicate last-digit-uncertainties.

	R_0 (wine) (s^{-1})	r (wine) s^{-1} (mg/L) $^{-1}$	r (H_2O solution) s^{-1} (mg/L) $^{-1}$
Mn^{2+}	0.467 (3)	0.155 (1)	0.126 [a]
Fe^{3+}	0.441 (8)	0.092 (4)	0.21 [b]; 0.1792 (4) [c]; 0.012*,0.019** [d]
Cu^{2+}	0.4591 (3)	0.0140 (2)	0.02 [e]; 0.014 [f]
Ni^{2+}	0.4867 (4)	0.0065 (1)	0.015 [g]; 0.010 [h]
Fe^{2+}	0.47 (1)	0.0075 (5)	0.008 [i]; 0.0065 [j]; 0.0067 [k]

[a] $MnCl_2$ N_2-degassed solution at 37 °C [80].
[b] $Fe(NO_3)_3$ in 1 M $HCL0_4$ [68].
[c] $FeCl_3$.6H20 solution, at 22 °C, pH = 1, ν_{Larmor} = 9.1 MHz [81].
[d] $FeCl_3$ or $Fe(NO_3)_3$, in 1.4 M HCl (*) or 5%HNO_3 (**), ν_{Larmor} = 60 MHz [58].
[e] $CuSO_4$ solution [82].
[f] From a NMRD profile [62].
[g] From Fig. 6 of Schlüter [55].
[h] $Ni(ClO_4)_2$ solution, pH 0.1–3, ν_{Larmor} = 12 MHz [83,84].
[i] $(NH_4)_2Fe(SO_4)_2$ solution at 37 °C, pH = 1 [85].
[j] Measured on fresh $FeSO_4{\cdot}7H_2O$ solution, in N2 degassed water (~0.5 mg/L of O_2) [86].
[k] From a NMRD profile of a 10 mM of $(NH_4)_2Fe(SO_4)_2$ [62].

big-size paramagnetic complexes (with sugars or organic acids), which is not observed in wine.

5.2. Manganese titration in wines.

In the following, we propose a method to quantify the manganese concentration in wines, in a simple model free approach. This is of interest for wine control or identification. The goal is to remove miscalculation due to other paramagnetic ions like Fe^{3+} but also R_0-contribution that, for many reasons, may vary from one wine to another. An illustration of such effects is presented in Fig. 4 where the relaxation rate of different model wines are reported versus the alcoholic strength of the solutions. It is worth noting that the linear dependence over the alcohol percent is no longer verified above ~40% in volume of alcohol [97].

Variation of the synthetic wine relaxation rate versus Mn^{2+} concentration for various Larmor frequencies is reported in Fig. 1S in the supplementary information. A linear dependence is confirmed for all frequencies and can be simply formalized as:

$$R_{\nu A} = b_{\nu A} + r_{\nu A}^{Mn}.C^{Mn} \quad (13)$$

where $R_{\nu A}$ stands for the relaxation rate at a Larmor frequency νA, $r_{\nu A}^{Mn}$, and $b_{\nu A}$ are the relaxivity and the intercept at νA, and C^{Mn} is the concentration of Mn^{2+}. The intercept (0.51 s^{-1}) shows little variations (± 0.02 s^{-1}), and it is convenient to assume it independent of the Larmor frequency and to associate it with the relaxation rate of the solvent R_0 when no manganese is present in the wine [52].

Equation (13) can be written as:

$$R_{\nu A} = R_0 + r_{\nu A}^{Mn}.C^{Mn} \quad (14)$$

Considering two points A and B on the wine profile we may extract the manganese concentration according to:

$$C^{Mn} = \frac{R_{\nu A} - R_{\nu B}}{r_{\nu A}^{Mn} - r_{\nu B}^{Mn}} \quad (15)$$

Equation (15) is in principle valid for any couple of frequency, and does only depend on the slopes of the titration lines at frequencies A and B. In particular, if we consider two points below roughly 1 MHz, and since R_D can reasonably be approximated to a constant value (Fig. 1) any dipolar contribution is cancelled in the numerator of equation (15) and this equation only quantifies the manganese involved in the contact interaction. All possible significant paramagnetic contributions from other nuclei (Cu^{2+}, Fe^{2+}, Fe^{3+}, Ni^{2+}) vanish. Moreover, by the same way, equation (15) does also eliminate the solvent contribution (R or R_0 in equation (1) or (14)) i.e., it is independent of chemical or physical properties that may give different intercepts from one wine to another. Consequently, equation (15) should allow for a straightforward and robust estimation of the manganese concentration within the samples. Fig. 5 illustrates the calculation for all possible frequency couples for a model wine containing 0.53 mg/L of Mn^{2+} (MW053).

Two areas of the contour plot give unsatisfactory results: (i) the diagonal zone for which two close frequencies are chosen and unsurprisingly the reliability decreases as frequencies come closer, (ii) a low frequency band (<0.02 MHz) for which the collected data are less reliable due to imperfect magnetic earth field compensation during the measurement. Couples of point taken from the two plateaus of the NMRD profile (in the ranges 0.02–0.06 and 1–3 MHz) are expected to give good results since relaxation rates are significantly different between the two ranges, whereas within each zone, the variation is smooth. This area corresponds to the square in Fig. 5, and is approximately situated in the middle of the grey area where all calculated concentrations are in the range 0.53 ± 0.02 mg/L. Indeed, the manganese concentration calculated with the 25 points in the square is 0.53 ± 0.01 mg/L, in agreement with the expected value of 0.53 mg/L. Even when the calculation zone extends to the dashed rectangle (120 points) and the triangle (300 points), concentrations are stable:

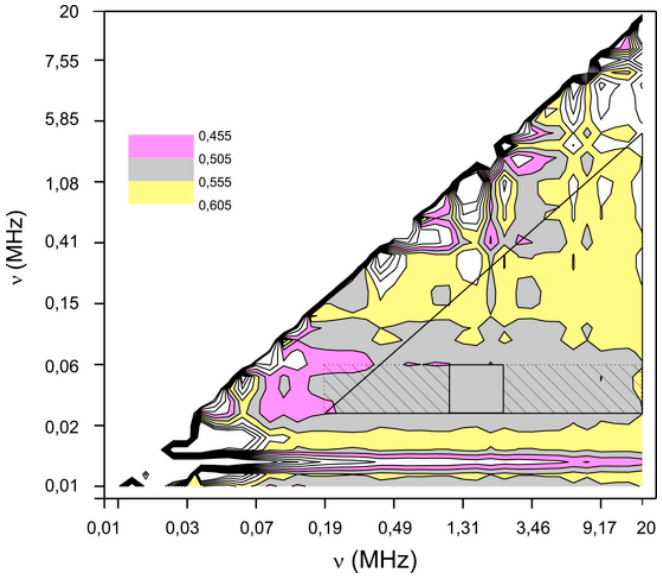

Fig. 5. Manganese concentration calculated on MW053. Only half of the symmetrical data is plotted. Color legend is expressed in mg/L and contour plot levels are drawn every 0.05 mg/L. Square, dashed rectangle and triangle are arbitrary zones for statistical calculations. No processing of the data (filtering, smoothing, or interpolation) is applied. (For interpretation of the references to color in this figure legend, the reader is referred to the Web version of this article.)

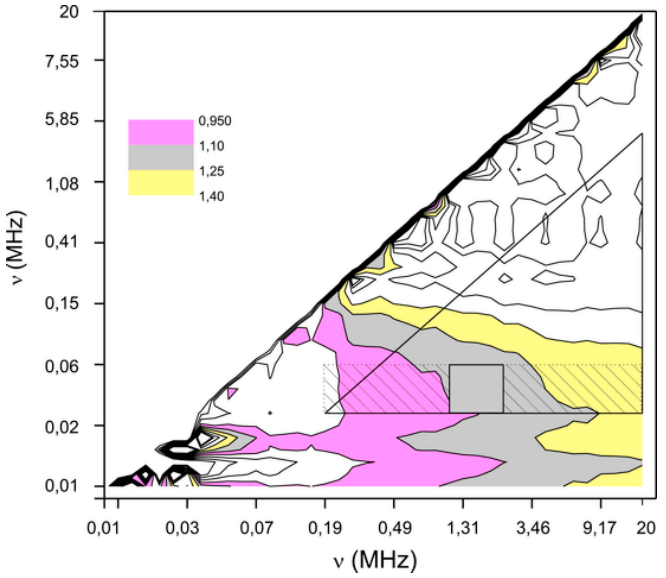

Fig. 6. Manganese concentration calculated on Wa. Color legend is expressed in mg/L and levels are uniformly represented with a 0.15 mg/L step. Square, rectangle and triangle are calculation zones consistent with Figure 5. No data processing is applied. (For interpretation of the references to color in this figure legend, the reader is referred to the Web version of this article.)

0.52 ± 0.01 and 0.53 ± 0.05 mg/L, respectively. Comparable results are obtained for all other model wines (Table 5).

The concentration contour plot of Wa reported in Fig. 6 presents similarities with Fig. 5: low and diagonal frequencies are subject to unstabilities. However, the calculated concentrations are more dispersed in Fig. 6, in particular for the higher frequencies of the triangular zone, and the plateau supporting the rectangular zone is not so well defined: concentrations are monotonously increasing along the x-axis.

Table 5
Calculated manganese concentration (mg/L) according to equation (15). In the square zone, 25 points are used for the statistical calculation, 120 and 300 points are considered in the rectangle and triangle zone, respectively. Samples Wa and Ra are recorded with different experimental condition but approximately the same zones have been chosen however, only 12, 72 and 171 experimental points are in the zones. Numbers in parenthesis indicate the standard deviation on the last digit.

	Manganese concentration	Square zone	Rectangular zone	Triangular zone
MW546	5.46	5.46 (3)	5.45 (4)	5.5 (1)
MW501	5.01	4.97 (5)	4.97 (6)	5.0 (1)
MW128	1.28	1.34 (8)	1.3 (1)	1.3 (1)
MW053	0.53	0.53 (1)	0.52 (1)	0.53 (5)
MW005	0.05	0.063 (5)	0.063 (6)	0.06 (1)
Wa	1.26 (2) [a]	1.17 (9)	1.2 (1)	1.3 (2)
Wb		1.13 (3)	1.1 (1)	1.4 (2)
EW	< 0.002 [a]	0.009 (6)	0.011 (4)	0.01 (1)
Ra	1.06 (2) [a]	0.83 (4)	0.9 (1)	1.2 (3)
Rb		0.91 (5)	0.9 (1)	1.2 (3)

[a] Concentration measured by ICP AES.

From square to triangle, the concentrations are calculated to be 1.17 ± 0.09, 1.2 ± 0.1 and 1.3 ± 0.2 mg/L (Table 5), in good agreement with the calculated concentration issued from the refinement of the low field dispersion.

While in the case of model wines, the three calculated concentrations were fairly consistent, for the real wines some variations are observed, particularly in the upper part of the triangle zone. We may attribute this deviation to the additional paramagnetic elements present in the wine. Even though other paramagnetic ions have a low relaxivity with respect to Mn^{2+} (Fig. 3), when couples of high frequencies are considered, the profile is mainly governed by the dipolar dispersion, and the cumulative dipolar contributions of other paramagnetic ions (Fe^{3+}, Cu^{2+},Ni^{2+}) may then be less negligible and result in an increase of the calculated manganese concentration. If one wishes to further analyze the results, it appears that the concentrations are slightly underestimated. This could be explained by the fact that on NMRD profiles, manganese complexation is particularly visible on the low field dispersion caused by the contact interaction, which induces a decrease of the relaxation rate [54,79]. Since wine has a high tendency for forming complexes with minor and trace-metal cations [5,17,98,99], we could attribute the manganese concentration deficit observed on the low field singularity to the complexation of Mn^{2+}. On overall, while manganese concentration is measured with very high accuracy on model wine, small differences remain between ICP-AES and relaxometric measurement performed on real wines. NMRD profiles may still contain unrevealed information.

Despite no manganese signature on the NMRD profile of the exchanged wine is visible, equation (15) is also applied to the exchanged wine sample, and reasonable concentrations of the order of 0.01 mg/L are obtained (ICP-AES analysis gives less than 0.002 mg/L (Table 5)).

6. Conclusions

NMR proton relaxation of wine clearly originates from paramagnetic ions naturally present in wine. In the samples studied the relaxation is governed by Mn^{2+} relaxation for which very low concentration (few tens of μg/L) can be quantify in situ with a good accuracy. Moreover, NMR relaxometry should also be able to reveal Fe^{3+} when present. The double dispersion signature of Mn^{2+} observed on proton profile allows in a model independent straightforward calculation for a simple and precise measurement of manganese concentration independently of all other paramagnetic ions, or solvent effect and could reveal manganese complexation. This approach is obviously not limited to wine and should be useable for various chemical solution, biological fluids, or gels.

Author Contributions

The manuscript was written through contributions of all authors. All authors have given approval to the final version of the manuscript. P.R.B. and A.R. performed the NMR experiments. B.M. performed the ICP analyses. J.T.G, R.D.G., T.K., and P.S-K. contributed to materials and analysis tools. P.R.B. and R.D.G wrote the communication.

Declaration of competing interest

The authors declare no competing financial interest.

Acknowledgements

Authors are grateful to COST Action CA15209 European Network on NMR Relaxometry (EURELAX) P.R.B. thanks Aymerick Batlogg for synthesizing and T1 measurements at 19.65 MHz of Fe-model wines as well as for the data of Fig. 4. Authors are very thankful to the referees for their valuable comments. This work was supported by the Regional council of Bourgogne Franche comté, France and the "Fonds Européen de Développe-

ment Régional (FEDER)". Graphical abstract based on a design by rawpixel.com/Freepik.

Appendix A. Supplementary data

Supplementary data to this article can be found online at https://doi.org/10.1016/j.talanta.2019.120561.

References

[1] H. Eschnauer, Spurenelemente in Wein und anderen Getrinken Weinheim, 1974.
[2] H. Eschnauer, Trace elements in must and wine: primary and secondary contents, Am. J. Enol. Vitic. 33 (1982) 226.
[3] C.M.R. Almeida, M.T.S.D. Vasconcelos, Multielement composition of wines and their precursors including provenance soil and their potentialities as fingerprints of wine origin, J. Agric. Food Chem. 51 (2003) 4788–4798, doi:10.1021/jf034145b.
[4] G. Nicolini, R. Larcher, P. Pangrazzi, L. Bontempo, Changes in the contents of micro- and trace-elements in wine due to winemaking treatments, Vitis 43 (2004) 41–45.
[5] P. Pohl, What do metals tell us about wine?, Trac. Trends Anal. Chem. 26 (2007) 941–949, doi:10.1016/j.trac.2007.07.005.
[6] M.G. Volpe, F. La Cara, F. Volpe, A. De Mattia, V. Serino, F. Petitto, C. Zavalloni, F. Limone, R. Pellecchia, P.P. De Prisco, M. Di Stasio, Heavy metal uptake in the enological food chain, Food Chem. 117 (2009) 553–560, doi:10.1016/j.foodchem.2009.04.033.
[7] H. Hopfer, J. Nelson, A.E. Mitchell, H. Heymann, S.E. Ebeler, Profiling the trace metal composition of wine as a function of storage temperature and packaging type, J. Anal. Atomic Spectrom. 28 (2013) 1288–1291, doi:10.1039/c3ja50098e.
[8] J.D. Greenough, H.P. Longerich, S.E. Jackson, Element fingerprinting of Okanagan Valley wines using ICP-MS: relationships between wine composition, vineyard and wine colour, Aust. J. Grape Wine Res. 3 (1997) 75–83, doi:10.1111/j.1755-0238.1997.tb00118.x.
[9] M.J. Baxter, H.M. Crews, M. John Dennis, I. Goodall, D. Anderson, The determination of the authenticity of wine from its trace element composition, Food Chem. 60 (1997) 443–450, doi:10.1016/S0308-8146(96)00365-2.
[10] P.P. Coetzee, F.E. Steffens, R.J. Eiselen, O.P. Augustyn, L. Balcaen, F. Vanhaecke, Multi-element analysis of South African wines by ICP–MS and their classification according to geographical origin, J. Agric. Food Chem. 53 (2005) 5060–5066, doi:10.1021/jf048268n.
[11] H. Hopfer, J. Nelson, T.S. Collins, H. Heymann, S.E. Ebeler, The combined impact of vineyard origin and processing winery on the elemental profile of red wines, Food Chem. 172 (2015) 486–496, doi:10.1016/j.foodchem.2014.09.113.
[12] J.C. Danilewicz, Fe(II):Fe(III) ratio and redox status of white wines, Am. J. Enol. Vitic. 67 (2016) 146–152, doi:10.5344/ajev.2015.15088.
[13] M. Rousseva, N. Kontoudakis, L.M. Schmidtke, G.R. Scollary, A.C. Clark, Impact of wine production on the fractionation of copper and iron in Chardonnay wine: implications for oxygen consumption, Food Chem. 203 (2016) 440–447, doi:10.1016/j.foodchem.2016.02.081.
[14] H. Eschnauer, L. Jakob, H. Meierer, R. Neeb, Use and limitations of ICP-OES in wine analysis, Microchimica Acta 99 (1989) 291–298, doi:10.1007/BF01244684.
[15] A.E. Martin, R.J. Watling, G.S. Lee, The multi-element determination and regional discrimination of Australian wines, Food Chem. 133 (2012) 1081–1089, doi:10.1016/j.foodchem.2012.02.013.
[16] D. Cozzolino, M.J. Kwiatkowski, R.G. Dambergs, W.U. Cynkar, L.J. Janik, G. Skouroumounis, M. Gishen, Analysis of elements in wine using near infrared spectroscopy and partial least squares regression, Talanta 74 (2008) 711–716, doi:10.1016/j.talanta.2007.06.045.
[17] M. Latorre, P. Herbello-Hermelo, C. Peña-Farfal, Y. Neira, P. Bermejo-Barrera, A. Moreda-Piñeiro, Size exclusion chromatography – inductively coupled plasma – mass spectrometry for determining metal-low molecular weight compound complexes in natural wines, Talanta 195 (2019) 558–565, doi:10.1016/j.talanta.2018.11.055.
[18] S. Kelly, K. Heaton, J. Hoogewerff, Tracing the geographical origin of food: the application of multi-element and multi-isotope analysis, Trends Food Sci. Technol. 16 (2005) 555–567, doi:10.1016/j.tifs.2005.08.008.
[19] S.A. Drivelos, C.A. Georgiou, Multi-element and multi-isotope-ratio analysis to determine the geographical origin of foods in the European Union, Trac. Trends Anal. Chem. 40 (2012) 38–51, doi:10.1016/j.trac.2012.08.003.
[20] E.P. Pérez-Álvarez, R. Garcia, P. Barrulas, C. Dias, M.J. Cabrita, T. Garde-Cerdán, Classification of wines according to several factors by ICP-MS multi-element analysis, Food Chem. 270 (2019) 273–280, doi:10.1016/j.foodchem.2018.07.087.
[21] N. Kontoudakis, L.M. Schmidtke, M.Z. Bekker, M. Smith, P.A. Smith, G.R. Scollary, E.N. Wilkes, A.C. Clark, Analytical strategies for the measurement of different forms of Cu and Fe in wine: comparison between approaches in relation to wine composition, Food Chem. 274 (2019) 89–99, doi:10.1016/j.foodchem.2018.08.084.
[22] D. Kruk, Theory of evolution and relaxation of multi-spin systems: application to nuclear magnetic resonance and electron spin resonance, arima publ, Bury St Edmunds (2007).
[23] R. Kimmich, NMR Tomography, Diffusometry, Relaxometry, Springer Berlin, Berlin, 2013.
[24] D. Kruk, Understanding Spin Dynamics, Pan Stanford Publishing, Singapore, 2016.
[25] A. Rachocki, L. Latanowicz, J. Tritt-Goc, Dynamic processes and chemical composition of Lepidium sativum seeds determined by means of field-cycling NMR relaxometry and NMR spectroscopy, Anal. Bioanal. Chem. 404 (2012) 3155–3164, doi:10.1007/s00216-012-6409-5.
[26] A. Rachocki, J. Tritt-Goc, Novel application of NMR relaxometry in studies of diffusion in virgin rape oil, Food Chem. 152 (2014) 94–99, doi:10.1016/j.foodchem.2013.11.112.
[27] P. Conte, V. Mineo, S. Bubici, C. De Pasquale, F. Aboud, A. Maccotta, D. Planeta, G. Alonzo, Dynamics of pistachio oils by proton nuclear magnetic resonance relaxation dispersion, Anal. Bioanal. Chem. 400 (2011) 1443–1450, doi:10.1007/s00216-011-4904-8.
[28] P. Conte, A. Maccotta, C.D. Pasquale, G. Alonzo, Supramolecular organization of triglycerides in extra-virgin olive oils as assessed by nmr relaxometry, Fresenius Environ. Bull. 19 (2010) 6.
[29] P. Conte, S. Bubici, E. Palazzolo, G. Alonzo, Solid-state ^{1} H-NMR relaxation properties of the fruit of a wild relative of eggplant at different proton larmor frequencies, Spectrosc. Lett. 42 (2009) 235–239, doi:10.1080/00387010902895038.
[30] R. Lo Scalzo, M. Fibiani, G. Francese, A. D'Alessandro, G.L. Rotino, P. Conte, G. Mennella, Cooking influence on physico-chemical fruit characteristics of eggplant (Solanum melongena L.), Food Chem. 194 (2016) 835–842, doi:10.1016/j.foodchem.2015.08.063.
[31] D. Capitani, A.P. Sobolev, M. Delfini, S. Vista, R. Antiochia, N. Proietti, S. Bubici, G. Ferrante, S. Carradori, F.R.D. Salvador, L. Mannina, NMR methodologies in the analysis of blueberries: General, Electrophoresis 35 (2014) 1615–1626, doi:10.1002/elps.201300629.
[32] M. Ladd-Parada, M.J. Povey, J. Vieira, M.E. Ries, Fast field cycling NMR relaxometry studies of molten and cooled cocoa butter, Mol. Phys. 117 (2019) 1020–1027, doi:10.1080/00268976.2018.1508784.
[33] M. Ladd Parada, M.J. Povey, J. Vieira, M. Rappolt, M.E. Ries, Early stages of fat crystallisation evaluated by low-field NMR and small-angle X-ray scattering, Magn. Reson. Chem. (2019), doi:10.1002/mrc.4860.
[34] M.I.B. Tavares, E.O. da Silva, P.S.R.C. Silva, P.J. Sebastião, The use of fast field cycling to evaluate the time domain relaxation of starches from tropical fruit seeds, Mol. Phys. 117 (2019) 1028–1033, doi:10.1080/00268976.2018.1540803.
[35] E. Curti, S. Bubici, E. Carini, S. Baroni, E. Vittadini, Water molecular dynamics during bread staling by Nuclear Magnetic resonance, LWT - Food Sci. Technol. (Lebensmittel-Wissenschaft -Technol.) 44 (2011) 854–859, doi:10.1016/j.lwt.2010.11.021.
[36] G. Cimo, P. Conte, Conformational redistribution of honey components following different storage conditions, Int. J. Spectrosc. (2015) 1–7, doi:10.1155/2015/354327.
[37] I. Płowaś-Korus, Ł. Masewicz, A. Szwengiel, A. Rachocki, H.M. Baranowska, W. Medycki, A novel method of recognizing liquefied honey, Food Chem. 245 (2018) 885–889, doi:10.1016/j.foodchem.2017.11.087.
[38] L. Laghi, M.A. Cremonini, G. Placucci, S. Sykora, K. Wright, B. Hills, A proton NMR relaxation study of hen egg quality, Magn. Reson. Imag. 23 (2005) 501–510, doi:10.1016/j.mri.2004.12.003.
[39] F. Bajd, A. Gradišek, T. Apih, I. Serša, Dry-cured ham tissue characterization by fast field cycling NMR relaxometry and quantitative magnetization transfer: FFC/qMT-NMR study of dry-cured hams, Magn. Reson. Chem. 54 (2016) 827–834, doi:10.1002/mrc.4462.
[40] S.S. Uguz, E.B. Ozvural, M.J. Beira, M.H. Oztop, P.J. Sebastião, Use of NMR Relaxometry to identify frankfurters of different meat sources, Mol. Phys. 117 (2019) 1015–1019, doi:10.1080/00268976.2018.1542162.
[41] S. Godefroy, J.-P. Korb, L.K. Creamer, P.J. Watkinson, P.T. Callaghan, Probing protein hydration and aging of food materials by the magnetic field dependence of proton spin-lattice relaxation times, J. Colloid Interface Sci. 267 (2003) 337–342, doi:10.1016/S0021-9797(03)00589-7.
[42] S. Baroni, R. Consonni, G. Ferrante, S. Aime, Relaxometric studies for food characterization: the case of balsamic and traditional balsamic vinegars, J. Agric. Food Chem. 57 (2009) 3028–3032, doi:10.1021/jf803727d.
[43] E. Anoardo, G. Galli, G. Ferrante, Fast-field-cycling NMR: applications and instrumentation, Appl. Magn. Reson. 20 (2001) 365–404.
[44] R. Kimmich, E. Anoardo, Field-cycling NMR relaxometry, Prog. Nucl. Magn. Reson. Spectrosc. 44 (2004) 257–320, doi:10.1016/j.pnmrs.2004.03.002.
[45] F. Noack, NMR field-cycling spectroscopy: principles and applications, Prog. Nucl. Magn. Reson. Spectrosc. 18 (1986) 171–276, doi:10.1016/0079-6565(86)80004-8.
[46] P. Benítez, R. Castro, C.G. Barroso, Removal of iron, copper and manganese from white wines through ion exchange techniques: effects on their organoleptic characteristics and susceptibility to browning, Anal. Chim. Acta 458 (2002) 197–202, doi:10.1016/S0003-2670(01)01499-4.
[47] J.H. Krepelka, B. Rejha, The anhydrous and the hydrated manganous sulphates.-part I, Collect. Czechoslov. Chem. Commun. 3 (1931) 517–535.
[48] S.G. Sinha, N.D. Deshpande, D.A. Deshpande, Dehydratation of crystalline MnSO4.4H2O, Thermochim. Acta 113 (1987) 95–104.
[49] A. Abragam, The Principles of Nuclear Magnetism, Reprinted, Oxford Univ. Press, Oxford, 2006.
[50] R. Kimmich, Field cycling in NMR relaxation spectroscopy: applications in biological, chemical and polymer physics, Bull. Magn. Reson. 1 (1980) 24.
[51] N. Bloembergen, E.M. Purcell, R.V. Pound, Relaxation effects in nuclear magnetic resonance absorption, Phys. Rev. 73 (1948) 679–712.
[52] S.H. Koenig, R.D. Brown, Field-cycling relaxometry of protein solutions and tissue: implications for MRI, Prog. Nucl. Magn. Reson. Spectrosc. 22 (1990) 487–567, doi:10.1016/0079-6565(90)80008-6.

[53] A. Schlüter, A. Weiss, Nuclear magnetic resonance relaxation titration, Fresenius' Z. Für Anal. Chem. 266 (1973) 177–186.
[54] A. Schlüter, A. Weiss, Nuclear magnetic relaxation rate as indicator in complexiметric titrations, Anal. Chim. Acta 99 (1978) 157–166.
[55] A. Schlüter, A. Weiss, Nuclear magnetic relaxation titration of Cu2+, Ni2+, Mn2+, Zn2+, and Fe3+ with 1, 10-phenanthroline hydrochloride in the presence of thiocyanate, Anal. Chim. Acta 97 (1978) 93–110.
[56] P.F. Cobra, B.F. Gomes, C.I.N. Mitre, L.L. Barbosa, L.V. Marconcini, L.A. Colnago, Measuring the solubility product constant of paramagnetic cations using time-domain nuclear magnetic resonance relaxometry, Microchem. J. 121 (2015) 14–17, doi:10.1016/j.microc.2015.02.002.
[57] B.F. Gomes, J.S. da S. Burato, C.M. Silva Lobo, L.A. Colnago, Use of the relaxometry technique for quantification of paramagnetic ions in aqueous solutions and a comparison with other analytical methods, Int. J. Anal. Chem. (2016) 1–5, doi:10.1155/2016/8256437.
[58] J. Sherwood, K. Lovas, Y. Bao, Development of an iron quantification method using nuclear magnetic resonance relaxometry, AIP Adv. 7 (2017), doi:10.1063/1.4977889 056728.
[59] F.V.C. Kock, M.P. Machado, G.P.B. Athayde, L.A. Colnago, L.L. Barbosa, Quantification of paramagnetic ions in solution using time domain NMR. PROS and CONS to optical emission spectrometry method, Microchem. J. 137 (2018) 204–207, doi:10.1016/j.microc.2017.10.013.
[60] I. Solomon, Relaxation processes in a system of two spins, Phys. Rev. 99 (1955) 559–565, doi:10.1103/PhysRev.99.559.
[61] N. Bloembergen, L.O. Morgan, Proton relaxation times in paramagnetic solutions. Effects of electron spin relaxation, J. Chem. Phys. 34 (1961) 842–850, doi:10.1063/1.1731684.
[62] I. Bertini, C. Luchinat, G. Parigi, 1H NMRD profiles of paramagnetic complexes and metalloproteins, Advances in Inorganic Chemistry, Elsevier, 2005, pp. 105–172, doi:10.1016/S0898-8838(05)57003-X.
[63] A.J. Pell, G. Pintacuda, C.P. Grey, Paramagnetic NMR in solution and the solid state, Prog. Nucl. Magn. Reson. Spectrosc. (2018), doi:10.1016/j.pnmrs.2018.05.001.
[64] S.H. Koenig, R.D. Brown, Relaxation of solvent protons by paramagnetic ions and its dependence on magnetic field and chemical environment: implications for NMR imaging, Magn. Reson. Med. 1 (1984) 478–495, doi:10.1002/mrm.1910010407.
[65] I. Bertini, M. Fragai, C. Luchinat, G. Parigi, Solvent 1H NMRD study of hexaaquochromium(III): inferences on hydration and electron relaxation, Inorg. Chem. 40 (2001) 4030–4035.
[66] L. Banci, I. Bertini, C. Luchinat, 1H NMRD studies of solutions of paramagnetic metal ions in ethyleneglycol, Inorg. Chim. Acta 100 (1985) 173–181, doi:10.1016/S0020-1693(00)88305-X.
[67] I. Bertini, F. Briganti, Z. Xia, C. Luchinat, Nuclear magnetic relaxation dispersion studies of hexaaquo Mn(II) ions in water-glycerol mixtures, J. Magn. Reson. Ser. A 101 (1993) 198–201.
[68] I. Bertini, F. Capozzi, C. Luchinat, Z. Xia, Nuclear and electron relaxation of Fe(OH2)63+, J. Phys. Chem. 97 (1993) 1134–1137.
[69] S.H. Koenig, C. Baglin, R.D. Brown, C. Fred Brewer, Magnetic field dependence of solvent proton relaxation induced by Gd3+ and Mn2+ complexes, Magn. Reson. Med. 1 (1984) 496–501, doi:10.1002/mrm.1910010408.
[70] J. Kowalewski, A. Egorov, D. Kruk, A. Laaksonen, S. Nikkhou Aski, G. Parigi, P.-O. Westlund, Extensive NMRD studies of Ni(II) salt solutions in water and water–glycerol mixtures, J. Magn. Reson. 195 (2008) 103–111, doi:10.1016/j.jmr.2008.08.011.
[71] P.L. Anelli, I. Bertini, M. Fragai, L. Lattuada, C. Luchinat, G. Parigi, Sulfonamide-functionalized gadolinium DTPA complexes as possible contrast agents for MRI: a relaxometric investigation, Eur. J. Inorg. Chem. (2000) 625–630, doi:10.1002/(SICI)1099-0682(200004)2000:4<625::AID-EJIC625>3.0.CO;2-2.
[72] P. Caravan, G. Parigi, J.M. Chasse, N.J. Cloutier, J.J. Ellison, R.B. Lauffer, C. Luchinat, S.A. McDermid, M. Spiller, T.J. McMurry, Albumin binding, relaxivity, and water exchange kinetics of the diastereoisomers of MS-325, a gadolinium(III)-Based magnetic resonance angiography contrast agent, Inorg. Chem. 46 (2007) 6632–6639, doi:10.1021/ic700686k.
[73] D.J. Mastarone, V.S.R. Harrison, A.L. Eckermann, G. Parigi, C. Luchinat, T.J. Meade, A modular system for the synthesis of multiplexed magnetic resonance probes, J. Am. Chem. Soc. 133 (2011) 5329–5337, doi:10.1021/ja1099616.
[74] M.W. Rotz, K.S.B. Culver, G. Parigi, K.W. MacRenaris, C. Luchinat, T.W. Odom, T.J. Meade, High relaxivity Gd(III)–DNA gold nanostars: investigation of shape effects on proton relaxation, ACS Nano 9 (2015) 3385–3396, doi:10.1021/nn5070953.
[75] I. Bertini, O. Galas, C. Luchinat, L. Messori, G. Parigi, A theoretical analysis of the 1H nuclear magnetic relaxation dispersion profiles of diferric transferrin, J. Phys. Chem. 99 (1995) 14217–14222, doi:10.1021/j100039a006.
[76] I. Bertini, C. Luchinat, K. Nerinovski, G. Parigi, M. Cross, Z. Xiao, A.G. Wedd, Application of NMRD to hydration of rubredoxin and a variant containing a (cys-S)3FeIII(OH) site, Biophys. J. 84 (2003) 545–551, doi:10.1016/S0006-3495(03)74873-5.
[77] C. Luchinat, G. Parigi, E. Ravera, Can metal ion complexes be used as polarizing agents for solution DNP? A theoretical discussion, J. Biomol. NMR 58 (2014) 239–249, doi:10.1007/s10858-013-9728-8.
[78] S. Aime, M. Botta, E. Terreno, Gd(III)-based contrast agent for MRI, Advances in Inorganic Chemistry, Elsevier, 2005, pp. 173–237, doi:10.1016/S0898-8838(05)57004-1.
[79] B. Drahoš, M. Pniok, J. Havlíčková, J. Kotek, I. Císařová, P. Hermann, I. Lukeš, É., Tóth, Mn2+ complexes of 1-oxa-4,7-diazacyclononane based ligands with acetic, phosphonic and phosphinic acid pendant arms: stability and relaxation studies, Dalton Trans. 40 (2011) 10131, doi:10.1039/c1dt10543d.
[80] W. Nordhøy, H.W. Anthonsen, M. Bruvold, P. Jynge, J. Krane, H. Brurok, Manganese ions as intracellular contrast agents: proton relaxation and calcium interactions in rat myocardium: manganese IN cardiac MRI, NMR Biomed. 16 (2003) 82–95, doi:10.1002/nbm.817.
[81] I. Mitreiter, S.E. Oswald, F. Stallmach, Investigation of iron (III)-release in the pore water of natural sands by NMR relaxometry, Open Magn. Reson. J. 3 (2010) 46–51.
[82] R.A. Bernheim, T.H. Brown, H.S. Gutowsky, D.E. Woessner, Temperature dependence of proton relaxation times in aqueous solutions of paramagnetic ions, J. Chem. Phys. 30 (1959) 950–956, doi:10.1063/1.1730133.
[83] H.G. Hertz, M. Holz, Longitudinal proton relaxation rates in aqueous Ni2+ solutions as a function of the temperature, frequency, and pH value, J. Magn. Reson. 63 (1969) 64–73, doi:10.1016/0022-2364(85)90153-2.
[84] J. Kowalewski, T. Larsson, P.-O. Westlund, Proton spin-lattice relaxation in aqueous solution of the nickel(II) ion, J. Magn. Reson. 74 (1969) 56–65, doi:10.1016/0022-2364(87)90078-3.
[85] J.C. Gore, Y.S. Kang, Measurement of radiation dose distributions by nuclear magnetic resonance (NMR) imaging, Phys. Med. Biol. 29 (1984) 1189–1197, doi:10.1088/0031-9155/29/10/002.
[86] A. Assifaoui, Personal Commun., (n.d.).
[87] A.W. Nolle, L.O. Morgan, Frequency dependence of proton spin relaxation in aqueous solutions of paramagnetic ions, J. Chem. Phys. 26 (1957) 642–648, doi:10.1063/1.1743361.
[88] R.J. Elias, A.L. Waterhouse, Controlling the fenton reaction in wine, J. Agric. Food Chem. 58 (2010) 1699–1707, doi:10.1021/jf903127r.
[89] J.C. Danilewicz, Reactions involving iron in mediating catechol oxidation in model wine, Am. J. Enol. Vitic. 64 (2013) 316–324, doi:10.5344/ajev.2013.12137.
[90] J.C. Danilewicz, Role of tartaric and malic acids in wine oxidation, J. Agric. Food Chem. 62 (2014) 5149–5155, doi:10.1021/jf5007402.
[91] G.Y. Kreitman, J.C. Danilewicz, D.W. Jeffery, R.J. Elias, Reaction mechanisms of metals with hydrogen sulfide and thiols in model wine. Part 2: iron- and copper-catalyzed oxidation, J. Agric. Food Chem. 64 (2016) 4105–4113, doi:10.1021/acs.jafc.6b00642.
[92] C. Roullier-Gall, M. Witting, F. Moritz, R.B. Gil, D. Goffette, M. Valade, P. Schmitt-Kopplin, R.D. Gougeon, Natural oxygenation of Champagne wine during ageing on lees: a metabolomics picture of hormesis, Food Chem. 203 (2016) 207–215, doi:10.1016/j.foodchem.2016.02.043.
[93] M. Nikolantonaki, P. Julien, C. Coelho, C. Roullier-Gall, J. Ballester, P. Schmitt-Kopplin, R.D. Gougeon, Impact of glutathione on wines oxidative stability: a combined sensory and metabolomic study, Front. Chem. 6 (2018), doi:10.3389/fchem.2018.00182.
[94] C. Coelho, P. Julien, M. Nikolantonaki, L. Noret, M. Magne, J. Ballester, R.D. Gougeon, Molecular and macromolecular changes in bottle-aged white wines reflect oxidative evolution–impact of must clarification and bottle closure, Front. Chem. 6 (2018), doi:10.3389/fchem.2018.00095.
[95] C. Roullier-Gall, B. Kanawati, D. Hemmler, G.K. Druschel, R.D. Gougeon, P. Schmitt-Kopplin, Electrochemical triggering of the Chardonnay wine metabolome, Food Chem. 286 (2019) 64–70, doi:10.1016/j.foodchem.2019.01.149.
[96] J.C. Danilewicz, P. Tunbridge, P.A. Kilmartin, Wine reduction potentials: are these measured values really reduction potentials?, J. Agric. Food Chem. 67 (2019) 4145–4153, doi:10.1021/acs.jafc.9b00127.
[97] E.V. Goldammer, M.D. Zeidler, Molecular motion in aqueous mixtures with organic liquids by nmr relaxation measurements, Ber. Bunsen Ges. Phys. Chem. 73 (1969) 4–15, doi:10.1002/bbpc.19690730105.
[98] P. Pohl, B. Prusisz, Chemical fractionation of Cu, Fe and Mn in canned Polish beers, J. Food Compos. Anal. 23 (2010) 86–94, doi:10.1016/j.jfca.2009.08.002.
[99] A.M. Green, G.R. Scollary, Influence of metal ions on lead complexation in wine, Aust. J. Grape Wine Res. 6 (2000) 197–202, doi:10.1111/j.1755-0238.2000.tb00179.x.